Plant Communications
Research Article

CellPress
Partner Journal

Bromodomain-containing subunits BRD1, BRD2, and BRD13 are required for proper functioning of SWI/SNF complexes in *Arabidopsis*

Kamila Jarończyk[1], Katarzyna Sosnowska[2], Adam Zaborowski[1,4], Piotr Pupel[3], Maria Bucholc[2], Ewelina Małecka[1], Nina Siwirykow[1], Paulina Stachula[1], Roksana Iwanicka-Nowicka[1,2], Marta Koblowska[1,2], Andrzej Jerzmanowski[1,2] and Rafał Archacki[1,2,*]

[1]Laboratory of Systems Biology, Faculty of Biology, University of Warsaw, 02-106 Warsaw, Poland

[2]Institute of Biochemistry and Biophysics PAS, 02-106 Warsaw, Poland

[3]Department of Plant Physiology, Genetics and Biotechnology, University of Warmia and Mazury in Olsztyn, 10-719 Olsztyn, Poland

[4]Present address: Max Planck Institute of Molecular Plant Physiology, 14476 Potsdam-Golm, Germany

***Correspondence: Rafał Archacki (rafa@ibb.waw.pl)**

https://doi.org/10.1016/j.xplc.2021.100174

ABSTRACT

SWI/SNF chromatin remodelers are evolutionarily conserved multiprotein complexes that use the energy of ATP hydrolysis to change chromatin structure. A characteristic feature of SWI/SNF remodelers is the occurrence in both the catalytic ATPase subunit and some auxiliary subunits, of bromodomains, the protein motifs capable of binding acetylated histones. Here, we report that the *Arabidopsis* bromodomain-containing proteins BRD1, BRD2, and BRD13 are likely true SWI/SNF subunits that interact with the core SWI/SNF components SWI3C and SWP73B. Loss of function of each single BRD protein caused early flowering but had a negligible effect on other developmental pathways. By contrast, a *brd* triple mutation (*brdx3*) led to more pronounced developmental abnormalities, indicating functional redundancy among the BRD proteins. The *brdx3* phenotypes, including hypersensitivity to abscisic acid and the gibberellin biosynthesis inhibitor paclobutrazol, resembled those of *swi/snf* mutants. Furthermore, the BRM protein level and occupancy at the direct target loci *SCL3*, *ABI5*, and *SVP* were reduced in the *brdx3* mutant background. Finally, a *brdx3 brm-3* quadruple mutant, in which SWI/SNF complexes were devoid of all constituent bromodomains, phenocopied a loss-of-function mutation in BRM. Taken together, our results demonstrate the relevance of BRDs as SWI/SNF subunits and suggest their cooperation with the bromodomain of BRM ATPase.

Key words: *Arabidopsis*, chromatin remodeling, SWI/SNF complex, gene regulation, bromodomain-containing proteins, BRD

Jarończyk K., Sosnowska K., Zaborowski A., Pupel P., Bucholc M., Małecka E., Siwirykow N., Stachula P., Iwanicka-Nowicka R., Koblowska M., Jerzmanowski A., and Archacki R. (2021). Bromodomain-containing subunits BRD1, BRD2, and BRD13 are required for proper functioning of SWI/SNF complexes in *Arabidopsis*. Plant Comm. **2**, 100174.

INTRODUCTION

Dynamic changes in chromatin accessibility mediated by ATP-dependent chromatin-remodeling complexes (remodelers) are crucial for proper transcriptional responses to developmental and environmental stimuli. SWI/SNF complexes are the most thoroughly studied remodelers in yeast, plants, and animals. They are multiprotein assemblies consisting of a central catalytic Snf2-type ATPase associated with major core subunits—homologs of yeast SNF5, SWI3, and SWP73 proteins—as well as a variable number of auxiliary subunits (Clapier and Cairns, 2009). While the ATPase provides energy for the remodeling process, other subunits are thought to participate in the assembly of the complex, the regulation of ATPase activity, and the recruitment of SWI/SNF to target loci (Clapier and Cairns, 2009; Ho et al., 2019). In both mammals and plants, SWI/SNF subunits are encoded by

Published by the Plant Communications Shanghai Editorial Office in association with Cell Press, an imprint of Elsevier Inc., on behalf of CSPB and CEMPS, CAS.

multiple genes, enabling the combinatorial assembly of variant forms of the complexes with distinct properties (Jerzmanowski, 2007; Kadoch and Crabtree, 2015). SWI/SNF remodelers have been found to be essential for the transcriptional control of key developmental processes in all studied eukaryotic organisms. In plants, they are necessary for correct cotyledon separation, floral patterning, leaf development, root stem cell niche maintenance, inflorescence architecture, and flowering initiation (Han et al., 2015; Ojolo et al., 2018). Analyses of *Arabidopsis* mutants have also suggested a role for SWI/SNF in the regulation of hormonal pathways, including those of gibberellins (GAs) and abscisic acid (ABA) (Reyes, 2014; Sarnowska et al., 2016).

A distinctive feature of SWI/SNF-type remodelers in yeast and animals is the presence in some of their subunits of a characteristic four-helix bundle known as the bromodomain. This motif forms part of the C-terminal fragment of Snf2 ATPases and also occurs in some of the auxiliary subunits. Importantly, the arrangement of bromodomains is different in the two evolutionarily conserved major classes of SWI/SNF complexes, known as BAF and PBAF. In mammalian BAF-like complexes, bromodomain-containing auxiliary subunits are either absent or contain a single bromodomain motif, whereas PBAF-like complexes contain an additional and distinctive BAF180 subunit with tandemly arranged multiple bromodomains (Mashtalir et al., 2018; Ho et al., 2019). Unlike yeast and animals, *Arabidopsis* does not possess genes encoding proteins with multiple bromodomains, perhaps reflecting the fact that the separation of SWI/SNF complexes into BAF- and PBAF-like classes either did not occur or has not been preserved in plants (Jerzmanowski, 2007). This led to the hypothesis that the functions of SWI/SNF remodelers that require multiple bromodomains may be fulfilled in plants by complexes that contain separate auxiliary subunits, each with a single bromodomain (Jerzmanowski, 2007). The demonstration that bromodomain-containing proteins BRD1, BRD2, and BRD13 co-purified with major subunits of *Arabidopsis* SWI/SNF complexes (Vercruyssen et al., 2014) suggested that the combination of different single bromodomain plant proteins could indeed represent functional analogs of yeast and animal proteins with multiple copies of this motif.

Bromodomains are capable of recognizing and specifically binding acetylated histones (Chandrasekaran and Thompson, 2007; Shen et al., 2007; Awad and Hassan, 2008; Filippakopoulos et al., 2012; Morrison et al., 2017; Zhao et al., 2018) and are therefore considered major factors that enable the targeting of SWI/SNF complexes to nucleosomes enriched in epigenetic acetylation marks. Surprisingly, given this fact, mutations affecting bromodomains are in general considerably less severe than mutations in the ATPase or other major core subunits (Elfring et al., 1998; Hohmann et al., 2016; Morrison et al., 2017; Ho et al., 2019). In accordance with this observation, *Arabidopsis* null mutants in BRM ATPase display a severe phenotype, including dwarfism, strong leaf curling, and sterility, whereas the *brm-3* mutant, in which the BRM protein is deprived of its bromodomain, has only mild phenotypic defects (Hurtado et al., 2006; Farrona et al., 2007). This suggests that bromodomains may only be required for selected functions of SWI/SNF complexes, while being dispensable for the majority of others, or, alternatively, that functional redundancy of bromodomains in different subunits may obscure their true roles in SWI/SNF complexes.

To examine the importance of bromodomains for SWI/SNF function, we characterized the *Arabidopsis* bromodomain-containing proteins BRD1, BRD2, and BRD13. We identified the major core subunits SWI3C and SWP73B as their direct interactors and further confirmed that BRD1, BRD2, and BRD13 are true auxiliary subunits of SWI/SNF complexes. Analyses of single, double, and triple *brd* mutants showed that BRD1, BRD2, and BRD13 act mostly redundantly to control vegetative development and flowering, as well as GA and ABA hormonal responses. When *brdx3* mutation was introduced into *brm-1*, the null mutant in BRM ATPase, the quadruple *brm-1 brdx3* mutants did not show any additive phenotypes, further supporting the notion that BRDs act in the same complex as BRM. Furthermore, the presence of BRD subunits is required for the maintenance of physiological BRM protein levels and BRM binding to its known target genes *SCL3*, *ABI5*, and *SVP*. Importantly, the triple *brd* mutation showed strong genetic interaction with the bromodomain-deficient hypomorphic BRM mutant *brm-3*. The *brd1 brd2 brd13 brm-3* quadruple mutant (*bromo4*), in which SWI/SNF complexes lack all bromodomains, displayed a severe phenotype that phenocopied the BRM *null* mutant. Our data thus demonstrate that the presence of at least one bromodomain is essential for major SWI/SNF functions in *Arabidopsis*.

RESULTS

Arabidopsis BRD1, BRD2, and BRD13 proteins are close homologs of mammalian bromodomain-containing SWI/SNF subunits

The *Arabidopsis* genome encodes 29 proteins containing a single bromodomain, including the canonical SWI/SNF ATPase subunit BRAHMA (BRM) (Knizewski et al., 2008; Pandey et al., 2002; Rao et al., 2014). Three of these proteins, BRD1 (AT1G20670), BRD2 (AT1G76380), and BRD13 (AT5G55040), were previously co-purified with the transcriptional coactivator ANGUSTIFOLIA3 (AN3) and the SWI/SNF core subunits SWI3C and SWP73B (Vercruyssen et al., 2014), suggesting that they may be true auxiliary components of *Arabidopsis* SWI/SNF complexes. To verify this possibility, we performed immunoprecipitation-mass spectrometry (IP/MS) analysis of proteins co-immunoprecipitated with BRM-GFP stably expressed under its native promoter in the *brm-1* null mutant background. BRD1, BRD2, and BRD13 were found among the identified proteins, together with major SWI/SNF core subunits and recently characterized BRIP1/2 proteins (Yu et al., 2020) (Figure 1A, supplemental Table 1 and supplemental Data 1). Comparative sequence analysis revealed that BRD1, BRD2, and BRD13 are closely related and form a single branch of the phylogenetic tree of bromodomain-containing proteins. Moreover, and importantly, they are more similar to the human SWI/SNF subunits BRD7 and BRD9 than to other *Arabidopsis* bromodomain proteins (Figure 1B). The amino acid sequences of BRD1 and BRD2 are 60% identical, and that of BRD13, which has a longer C-terminal part, is 45% and 41% identical to BRD1 and BRD2, respectively. However, the bromodomain sequences are 90%, 72%, and 69% identical between BRD1 and BRD2, BRD1 and BRD13, and BRD2 and BRD13, respectively (Figure 1C). In addition to the conserved bromodomain, all three BRDs possess one or more coiled-coil domains (Figure 1D)—a structural motif

A

IP: BRM-GFP										
SWI/SNF subunit	SWI3C	SWP73B	SWP73A	ARP4	ARP7	BRIP1	BRIP2	BRD1	BRD2	BRD13
No. of replicates	3/3	3/3	1/3	3/3	3/3	1/3	3/3	3/3	2/3	3/3

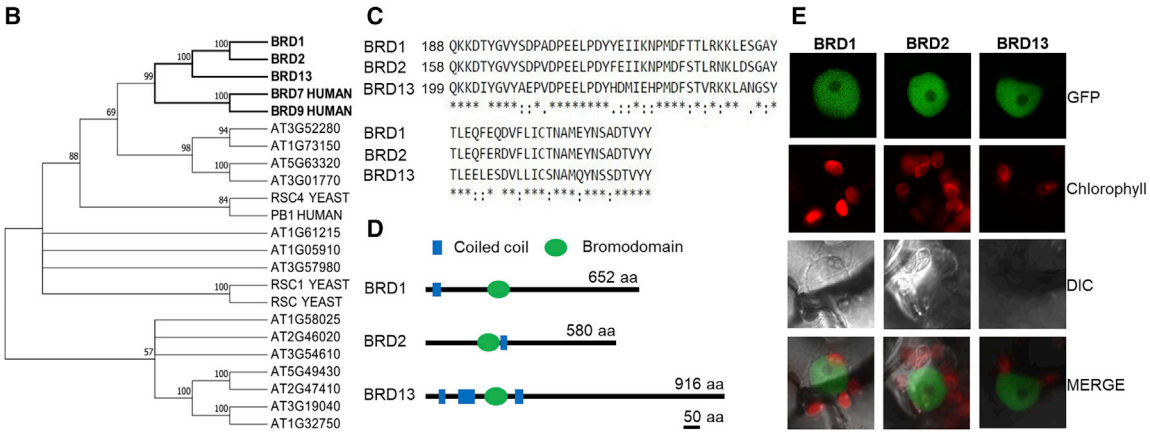

Figure 1. *Arabidopsis* BRD1, BRD2, and BRD13 proteins are closely related and form a separate family.

(A) Known SWI/SNF subunits and the three BRD proteins co-purified with BRM-GFP from 14-day-old *Arabidopsis* seedlings. The numbers of identifications in total from three biological replicates are shown.

(B) Phylogenetic tree of *Arabidopsis* bromodomain-containing proteins and their yeast and human homologs. *Arabidopsis* BRD1, BRD2, and BRD13, other representative *Arabidopsis* BRD proteins, and yeast and human SWI/SNF subunits containing bromodomains were used in the analysis.

(C) Alignment of the amino acid sequences of BRD1, BRD2, and BRD13 that correspond to the bromodomain. Numbers indicate the position of the first amino acid (glutamine) in each bromodomain. Identical amino acids in all three BRDs are marked by asterisks.

(D) Domain architecture of BRD1, BRD2, and BRD13. Each BRD contains a single bromodomain and one to three coiled-coil motifs.

(E) Nuclear localization of BRD-GFP fusions transiently expressed in tobacco epidermal cells examined by laser scanning confocal microscopy. DIC, differential interference contrast.

involved in protein-protein interactions that play important roles in major cellular processes (Truebestein and Leonard, 2016). Consistent with their association with SWI/SNF complexes, the three *Arabidopsis* BRDs displayed nuclear localization when transiently expressed in tobacco epidermal cells (Figure 1E). Together, the results of IP/MS experiments, comparative sequence analyses, and *in vivo* cellular localization studies provide strong support for the notion that *Arabidopsis* SWI/SNF complexes include non-ATPase bromodomain-containing subunits.

BRD1, BRD2, and BRD13 proteins directly interact with major core subunits of the *Arabidopsis* SWI/SNF complex

To test whether the studied BRD proteins can directly interact with canonical components of SWI/SNF complexes, we first used yeast two-hybrid (Y2H) analysis to examine interactions between BRD1 and a set of known *Arabidopsis* SWI/SNF core subunits: two ATPases (BRM and SYD), four SWI3 subunits (SWI3A-D), two SWP73 subunits (SWP73A and B), two ARP subunits (ARP4 and ARP7), and BSH. Of the 11 interactions tested, BRD1 was found to bind the SWI3C and SWP73B subunits (supplemental Figure 1A). We next showed that the other two BRD proteins, BRD2 and BRD13, also directly interacted with SWI3C and SWP73B (Figure 2A and supplemental Figure 1B). Physical interaction between all three BRDs and SWI3C was further confirmed *in planta* using a bimolecular fluorescence complementation (BiFC) assay. Tobacco epidermal cells expressing each of the three BRD proteins and SWI3C fused to complementary fragments of yellow fluorescent protein showed a clear YFP fluorescence signal in the nucleus (Figure 2B). We concluded that BRD1, BRD2, and BRD13 are all capable of direct physical interaction with core subunits of the *Arabidopsis* SWI/SNF complex in living plant cells.

We next determined which domains of BRD1 are involved in the interaction with SWI3C. Two N-terminal fragments, BRD1-N1 (amino acids 1–140) and BRD1-N2 (amino acids 1–294), did not interact with this subunit, whereas two fragments containing the C-terminal regions BRD1-C1 (amino acids 69–653) and BRD1-C2 (amino acids 289–653) were both able to interact with it (Figure 2C). This result demonstrates that the C-terminal region of BRD1, but not its coiled-coil or bromodomain motifs, is responsible for interactions with SWI3C.

Subunits SWI3C and SWP73B enable the incorporation of two BRD proteins into SWI/SNF complexes

To further explore interactions between BRDs and the core subunits of the SWI/SNF complex, we performed Y3H analyses. First, we investigated whether SWI3C can bind only one BRD or two different BRDs simultaneously. To this end, we expressed SWI3C fused to the activation domain of Gal4 (SWI3C/AD) and BRD13 fused to the DNA-binding domain of Gal4 (BRD13/BD), with or without the co-expression of BRD1 from a third plasmid (p426). Yeast growth was inhibited by the expression of BRD1 (Figure 3A), indicating that BRD1 and BRD13 compete for binding to SWI3C rather than binding simultaneously (Figure 3B). A similar analysis using SWP73B instead of SWI3C showed that SWP73B can also bind only one BRD protein (supplemental Figure 2A and 2B). The BRD1 protein did not

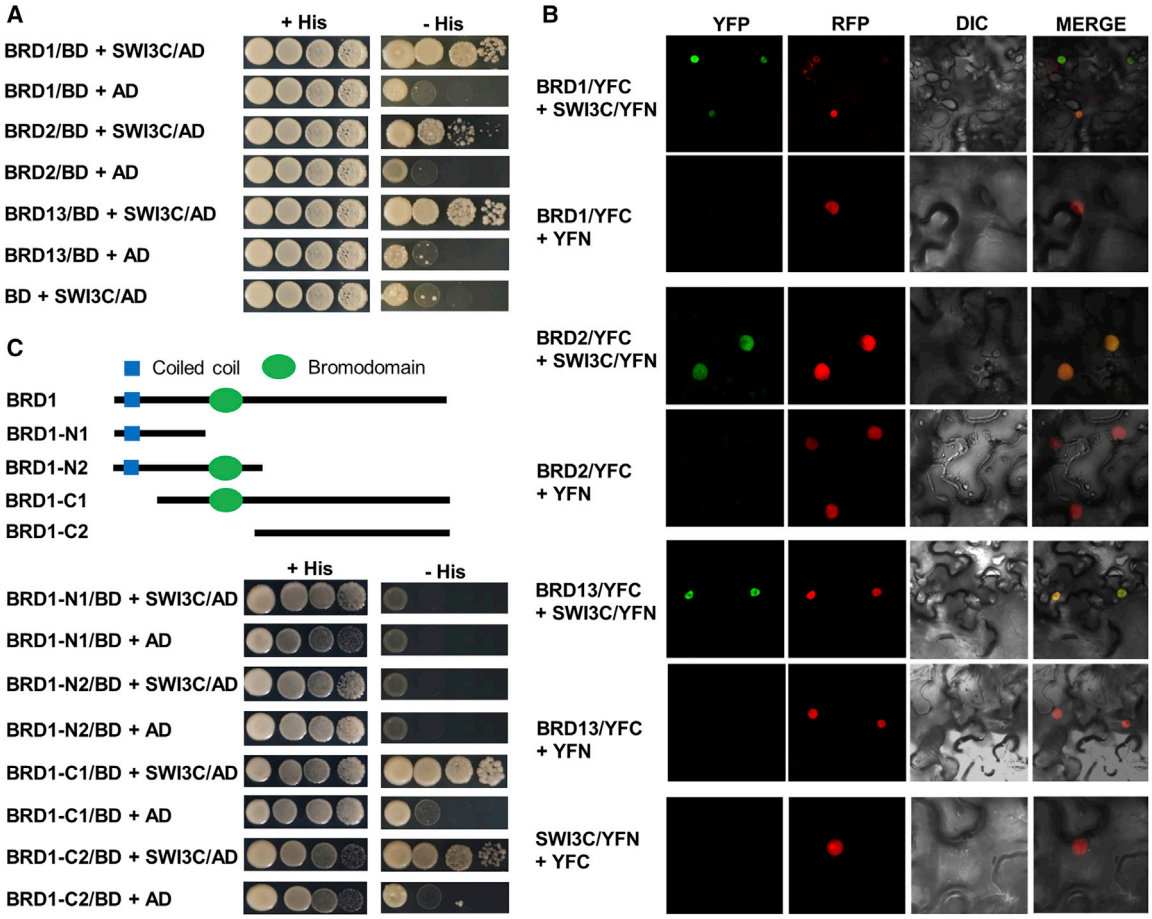

Figure 2. BRD1, BRD2, and BRD13 interact with the SWI/SNF core subunit SWI3C.

(A) Yeast two-hybrid assays showing interactions between bromodomain-containing proteins (BRD1, BRD2, and BRD13) and SWI3C. Serial 10-fold dilutions of yeast cell suspensions were plated onto medium with or without histidine (selection marker). BRD2 shows weaker interaction with SWI3C than BRD1 and BRD13.

(B) BRD1, BRD2, and BRD13 interact *in planta* with the SWI/SNF core subunit SWI3C. Bimolecular fluorescence complementation shows the interaction of BRD1 or BRD13 with SWI3C in the nuclei of tobacco leaf cells. To visualize nuclei, the cells were co-transformed with a plasmid expressing H2B-RFP.

(C) Domain analysis of BRD1 using yeast two-hybrid (Y2H) assays. The upper panel shows BRD1 and its truncated derivatives. Assays were performed as in **(A)**.

interact with BRD13 in these assays (supplemental Figure 1A and 2C). Consistent with the interaction of SWI3C with only one BRD, the expression of SWI3C did not improve the growth of yeast transformed with BRD1/AD and BRD13/BD, indicating that a BRD1-SWI3C-BRD13 ternary complex was not formed (supplemental Figure 2C).

Next, we used a Y3H assay to test whether SWI3C can simultaneously bind a BRD protein and another SWI/SNF core subunit. We expressed BRD1 fused to the activation domain of Gal4 (BRD1/AD) and SWP73A fused to the DNA-binding domain of Gal4 (SWP73A/BD), with or without the co-expression of SWI3C from a third plasmid (p426). We chose SWP73A (a second *Arabidopsis* ortholog of the SWP73 subunit) because it does not show interaction with BRD1 (supplemental Figure 1A) but interacts with SWI3C (Sacharowski et al., 2015), allowing easy detection of a potential ternary complex. As a result of interaction with SWI3C, the SWP73A/BD and BRD1/AD proteins would be placed in close proximity, thus resulting in activation of the His reporter and the promotion of yeast growth. Yeast transformed with the BRD1/AD and SWP73A/BD expression plasmids and empty p426 did not grow. However, growth was restored by the expression of SWI3C (Figure 3C), indicating that SWI3C can simultaneously and stably bind to both SWP73A and BRD1 (Figure 3D). A similar result was obtained when BRD13 was used instead of BRD1 (supplemental Figure 3A). We also found that the expression of BRD1 did not inhibit the SWI3C-SWP73B interaction, confirming that SWI3C and SWP73B are capable of interacting with each other and with BRDs (supplemental Figure 3B). These results support the notion that the subunits SWI3C and SWP73B together enable the simultaneous binding of two BRD proteins (either identical or different) to SWI/SNF complexes *in vivo*.

Characterization of *brd* mutants

We used available T-DNA insertion lines to investigate the functions of *BRD* genes in *Arabidopsis*. Following initial analyses of different mutant alleles (see Methods), we selected two mutant lines for each of the *BRD* genes for further characterization:

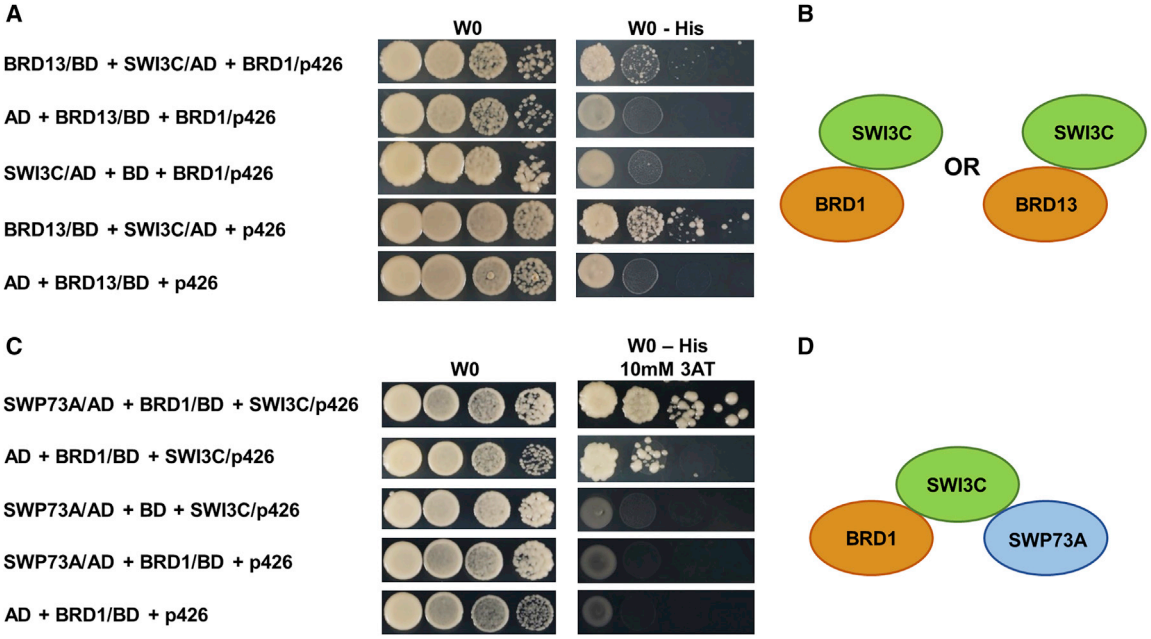

Figure 3. SWI3C can simultaneously bind one BRD and a core SWI/SNF subunit.

(A) Y3H growth assays showing interactions between SWI3C/AD and BRD13/BD in the presence or absence of BRD1. BRD13 was expressed as a fusion with the DNA-binding domain of Gal4 (BRD1/BD), and SWI3C was fused with the activation domain of Gal4 (SWI3C/AD). Serial 10-fold dilutions of yeast cell suspensions were plated onto medium with or without histidine. Upon the expression of BRD1 from vector p426, the reporter gene was not activated and the growth of the yeast cells was inhibited, indicating that BRD1 competes with BRD13 for binding to SWI3C.

(B) SWI3C binds either BRD1 or BRD13.

(C) Interactions of SWI3C, SWP73A, and BRD1. BRD1 was expressed as a fusion with the DNA-binding domain of Gal4 (BRD1/BD), and SWP73A was fused with the activation domain of Gal4 (SWP73A/AD). Serial 10-fold dilutions of yeast cell suspensions were plated onto medium with histidine or without histidine plus 3-AT. Upon expression of SWI3C from vector p426, the reporter gene was activated and the growth of the yeast cells was restored, indicating the formation of a complex consisting of these three proteins. Note that the expression of BRD1/BD + SWI3C can restore yeast growth to some extent, indicating that the BRD1-SWI3C dimer has some potential to activate transcription of the reporter gene.

(D) SWI3C can bind both SWP73A and BRD1 within the SWI/SNF complex.

brd1-2, *brd1-5*, *brd2-1*, *brd2-2*, *brd13-3*, and *brd13-4* (Figure 4A). Analysis of *BRD* expression in homozygous T-DNA lines revealed drastic reductions in transcript levels downstream of the insertions in *brd2* and *brd13* lines and a partial (two- to three-fold compared with the wild type [WT]) reduction in *brd1* lines (supplemental Figure 4). However, we were unable to detect full-length transcripts in any of the mutant lines (Figure 4B). Thus, because *brd1-2*, *brd1-5*, *brd2-1*, *brd2-2*, *brd13-3*, and *brd13-4* are likely null mutant alleles, we will hereafter refer to these mutants as *brd1*, *brd2*, and *brd13*.

The *brd1*, *brd2*, and *brd13* mutants were indistinguishable from WT plants up to 14 days of vegetative growth under standard conditions (long day [LD]) in a greenhouse. After this time, *brd13* plants could be distinguished, as their third and fourth leaves showed slight downward curling compared with corresponding leaves in the WT (supplemental Figure 5A), whereas *brd1* and *brd2* plants maintained a WT-like phenotype. Despite their weak or absent vegetative phenotypes, all three single *brd* mutants flowered earlier than WT plants (Figure 4C). Under LD conditions (16 h light/8 h dark), *brd1* and *brd2* bolted 3 and 2 days earlier with about 12 and 13 leaves, respectively, compared with the WT, which bolted after producing an average of 14 leaves (Figure 4E and 4F). This early flowering phenotype was weaker in *brd13* than in *brd1* and *brd2* mutants (Figure 4E and 4F); however, the difference in days to flowering between *brd13* and WT was statistically significant. Under short-day (SD) conditions (8 h light/16 h dark), *brd1* and *brd2* bolted 14 and 9 days earlier than the WT, respectively, after producing about six to seven fewer rosette leaves. Again, *brd13* showed a weaker flowering phenotype than *brd1* and *brd2*: it bolted with about four fewer leaves and 7 days earlier than the WT, and both differences were statistically significant (supplemental Figure 6). Together, these results indicate that BRDs act as repressors of flowering under both LD and SD conditions. The stronger flowering phenotypes observed in *brd1* and *brd2* compared with *brd13* suggest that BRD1 and BRD2 contribute more to the regulation of flowering time than does BRD13.

The overall similarity of the BRD proteins and the minor phenotypic alterations at the vegetative stage observed in single *brd* mutants indicate that the BRDs are functionally redundant. Consistent with this suggestion, the expression patterns of the *BRD* genes in available transcript profiling data and analyzed by RT-qPCR in this study are very similar in most organs and developmental stages. The highest transcript levels are present in seeds and embryos, shoot apical meristems, and floral organs (supplemental Figure 7). Double and triple mutant lines were constructed to assess the extent of redundancy between the *BRD* genes. We did not observe any additional phenotypic changes during vegetative development in the double mutants

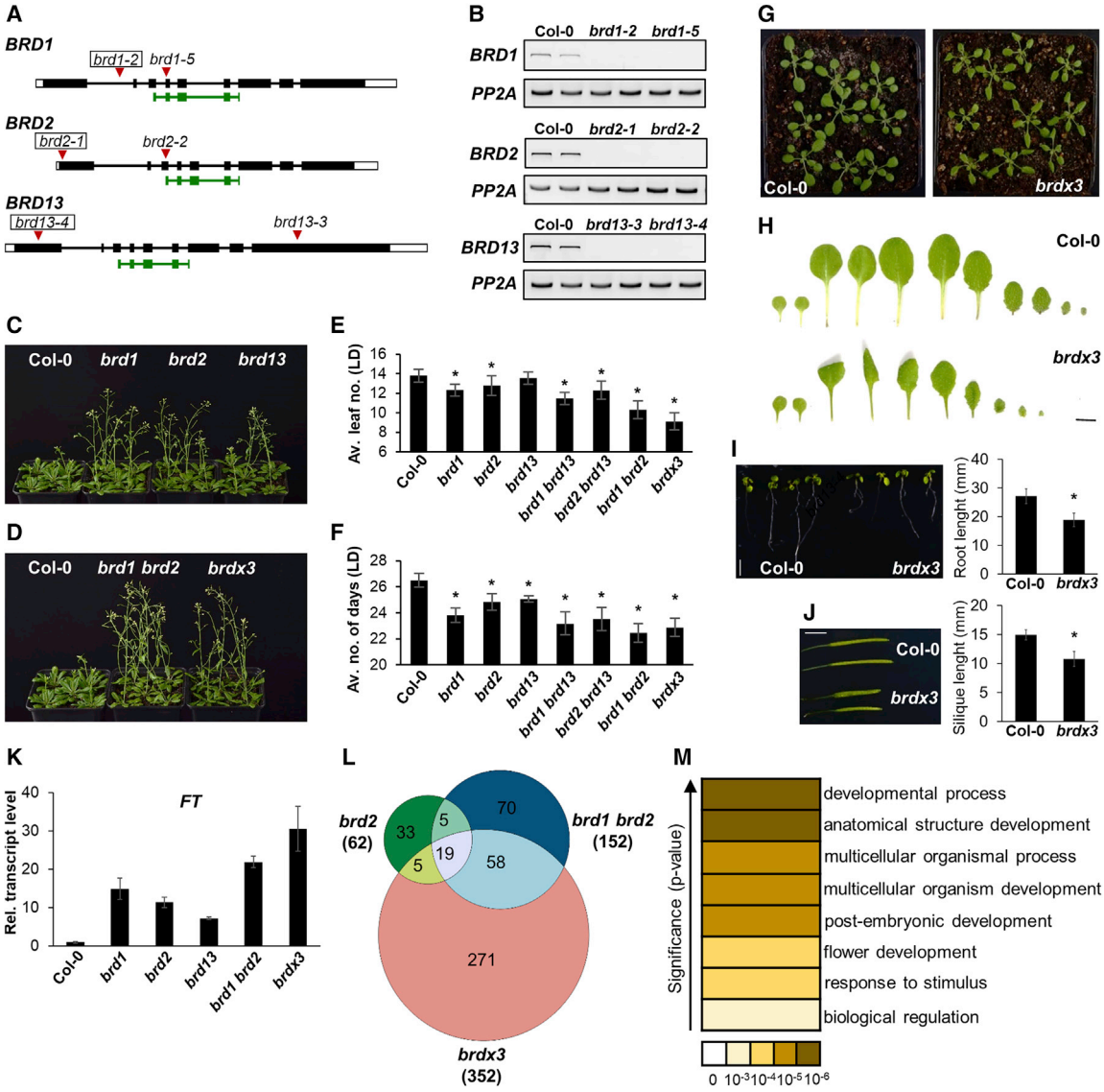

Figure 4. Characterization of *brd* mutants.

(A) Positions of T-DNA insertions in the *BRD* genes of mutant *Arabidopsis* lines. The regions encoding the predicted bromodomain in each gene are indicated below in green. The mutant alleles used to generate double and triple *brd* mutants are marked by rectangles.

(B) *BRD* transcripts detected in the mutant lines by RT–PCR. Total RNA was isolated from 15-day-old seedlings grown under LD conditions.

(C and D) WT and *brd* mutant plants flowering under LD conditions. Pictures were taken on the 36th day of growth.

(E and F) Leaf number at flowering and flowering time under LD conditions. Values are the mean ± STD. Asterisks indicate significant differences between the WT and mutant lines (Student's *t*-test, $P < 0.01$).

(G) WT and *brdx3* mutant plants at the rosette stage. Pictures were taken on the 18th day of growth under LD conditions.

(H) Leaf series of 18-day-old WT and *brdx3* plants grown under LD conditions.

(I) Roots of 10-day-old WT and *brdx3* plants.

(J) Siliques of WT and *brdx3* plants. Scale bars, 5 mm.

(K) *Flowering Locus T* (*FT*) transcript levels. RT-qPCR was performed using total RNA isolated from 15-day-old seedlings. The housekeeping gene *PP2A* was used as the normalization control. Transcript levels in the WT are set to 1. Error bars indicate the STD of three independent biological replicates.

(L) Venn diagram of differentially expressed genes identified in microarray data from the *brd2*, *brd1 brd2*, and *brd1 brd2 brd13* (*brdx3*) mutants.

(M) Gene ontology analysis of the panel of genes mis-expressed in the *brdx3* mutant, showing significantly enriched biological processes. The color gradient indicates increasing statistical significance.

brd1 brd13 and *brd2 brd13* compared with single mutants or WT plants, except for slightly enhanced leaf curvature. However, the early flowering phenotype was more pronounced in these double mutants. The effects of the mutations were additive, with the *brd1 brd2* mutant showing the greatest change: under LD conditions, it bolted an average of 4 days earlier than the WT with about 10 leaves, compared with about 14 leaves in the WT (Figure 4D–4F). Under SD conditions, *brd1 brd2* bolted an average of 20 days earlier than the WT and produced about 19 fewer rosette leaves (supplemental Figure 6). The flowering behavior

of the triple *brd1 brd2 brd13* (*brdx3)* mutant was similar to that of the double *brd1 brd2* mutant under both LD and SD conditions (Figure 4D–4F and supplemental Figure 6), confirming that *BRD1* and *BRD2* play a more important role than *BRD13* in the regulation of flowering time.

Except for similar flowering behavior, the *brdx3* triple mutant differed considerably from the single and double mutants. It displayed numerous developmental defects, consistent with BRD1, BRD2, and BRD13 acting mostly redundantly during development. Compared with the single and double mutants, *brdx3* plants were generally smaller (supplemental Figure 5B) and produced smaller and more curled leaves (Figure 4G and 4H) and shorter roots (Figure 4I). They developed flowers with a reduced number of stamens (5.4 ± 0.6 compared with 6.0 ± 0 in WT plants), occasional fusion of stamen filaments (5%–10% of flowers), and shorter siliques (Figure 4J) with a reduced number of seeds. Interestingly, these *brdx3* phenotypes resembled some features displayed by mutants in *BRM* and *SWI3C*, genes that encode two major core subunits of the SWI/SNF complex (Farrona et al., 2007; Hurtado et al., 2006; Sarnowski et al., 2005). We therefore introduced *brdx3* mutation into *brm-1*, a null mutant in the BRM ATPase. Quadruple *brm-1 brdx3* mutants did not show any additive phenotypes and were indistinguishable from *brm-1* (supplemental Figure 8), further supporting the notion that BRD1, BRD2, and BRD13 act as bona fide SWI/SNF subunits. Moreover, the expression of *BRD2* and *BRD13* was strongly elevated in *brm-1* (supplemental Figure 9), indicating a feedback regulatory mechanism by which the SWI/SNF complex can regulate the expression of some of its subunits. The upregulation of *BRD2* transcript level was also reported previously for the *brm-101* mutant (Bezhani et al., 2007).

Flowering regulatory genes are mis-expressed in *brd* mutants

To gain some insight into the possible causes of the early flowering behavior of *brd* mutants, we analyzed the expression of several major flowering regulators in 15-day-old seedlings. The transcript levels of the *FLOWERING LOCUS T* (*FT*) and *FRUITFULL* (*FUL*) genes were significantly increased in all *brd* mutants, whereas those of *CO*, *FD*, and *SOC1* were increased only slightly or remained unchanged (Figure 4K and supplemental Figure 10A). In agreement with the flowering phenotypes of the *brd* mutants, these changes in flowering regulator expression were additive and most pronounced in the double *brd1 brd2* and triple *brdx3* mutant plants (Figure 4K and supplemental Figure 10A). Strong upregulation of *FT* was also detected in 4-week-old *brd1 brd2* and *brdx3* mutants grown under SD conditions (supplemental Figure 10B), suggesting a possible causative role of *FT* mis-expression in the early flowering behavior of *brd* mutants under both LD and SD conditions. Upregulation of *FT* was also reported previously in the *brm-1* mutant (Farrona et al., 2011). In addition, in *brm-1*, the transcript levels of flowering repressors *FLC* and *SVP* were shown to be up- and downregulated, respectively (Farrona et al., 2011; Li et al., 2015). We therefore checked the abundance of *FLC* and *SVP* transcripts in WT and *brdx3* seedlings. We observed an increase in *FLC* expression and a reduction in *SVP* expression in *brdx3* compared with WT (supplemental Figure 10C) and concluded that BRDs regulate flowering transcriptionally in a manner similar to that of BRM.

BRDs regulate genes involved in development and responses to environmental stimuli

To investigate the effect of disruption of *BRD* genes on global gene expression in *Arabidopsis*, we performed transcriptome profiling of 18-day-old single *brd2*, double *brd1 brd2*, and triple *brdx3* mutants. Consistent with the demonstrated redundancy of *BRD* genes, this analysis showed an increasing number of mis-regulated genes in the single *brd2* (62 genes), double *brd1 brd2* (152 genes), and triple *brdx3* mutants (352 genes, 209 upregulated and 143 downregulated) compared with WT plants (Figure 4L, supplemental Figure 11A and 11B, and supplemental Data 2). Gene ontology (GO) analysis of mis-regulated genes in the *brdx3* mutant revealed significant enrichment of terms related to development and responses to stimuli (Figure 4M). Among the panel of mis-expressed genes were several flowering regulatory genes. Two of these, *FT* and *FUL*, were upregulated in all tested mutant lines, including the *brd2* single mutant (supplemental Data 2), consistent with the early flowering behavior of the *brd* mutants and with the RT-qPCR data (Figure 4K and supplemental Figure 10). Within the GO "development" categories, a number of key regulators of meristem and leaf development were found, including *STM*, *KNAT1*, *ARF4*, *KAN3*, and *YAB5*. Notably, *KAN3* and *YAB5* were mis-expressed in *brd1 brd2* and *brdx3* but not in the *brd2* single mutant (supplemental Data 2), which correlates with the leaf phenotypes of these mutants. Similar GO categories were previously shown to be mis-regulated in mutants of other SWI/SNF subunits such as BRM and SWP73B (Sacharowski et al., 2015; Archacki et al., 2017), implying that BRDs participate in SWI/SNF-mediated transcriptional regulation of these processes. We therefore compared the transcriptional profile of *brdx3* with our previously published data for the *brm-1* mutant obtained using similar growth conditions (Buszewicz et al., 2016). This analysis revealed that about 35% of genes mis-expressed in *brdx3* were also mis-regulated in *brm-1* mutants (supplemental Figure 11C). In addition, over 90% of the overlapping genes showed expression changes in the same direction (either up- or downregulation in both mutants, supplemental Figure 11C), an effect that would be expected for mutants in genes that encode subunits of the same complex.

BRDs are involved in ABA and GA hormonal responses

In plants, SWI/SNF complexes are required for the correct functioning of hormonal pathways, including those of ABA and GAs, as demonstrated by altered responses to these hormones of mutants in SWI/SNF core subunits (Archacki et al., 2013; Han et al., 2012; Sarnowska et al., 2016). For example, mutants in the *BRM* and *SWI3C* genes are both hypersensitive to treatment with ABA and PAC (paclobutrazol, an inhibitor of GA biosynthesis) (Archacki et al., 2013; Han et al., 2012). We therefore examined the responses of the *brdx3* triple mutant to ABA and PAC. *Brdx3* plants were hypersensitive to ABA, as indicated by inhibition of cotyledon expansion and greening (Figure 5A and 5B). The suppressive effects of ABA on growth were stronger in *brdx3* plants than in the *brm-3* hypomorphic mutant, in which ABA responses were previously characterized (Figure 5A and 5B) (Han et al., 2012). Moderate ABA-hypersensitive phenotypes were also observed in *brd* single mutants (supplemental Figure 12A). We next checked whether the observed phenotypes of *brdx3* correlated with changes in the expression of ABA-responsive

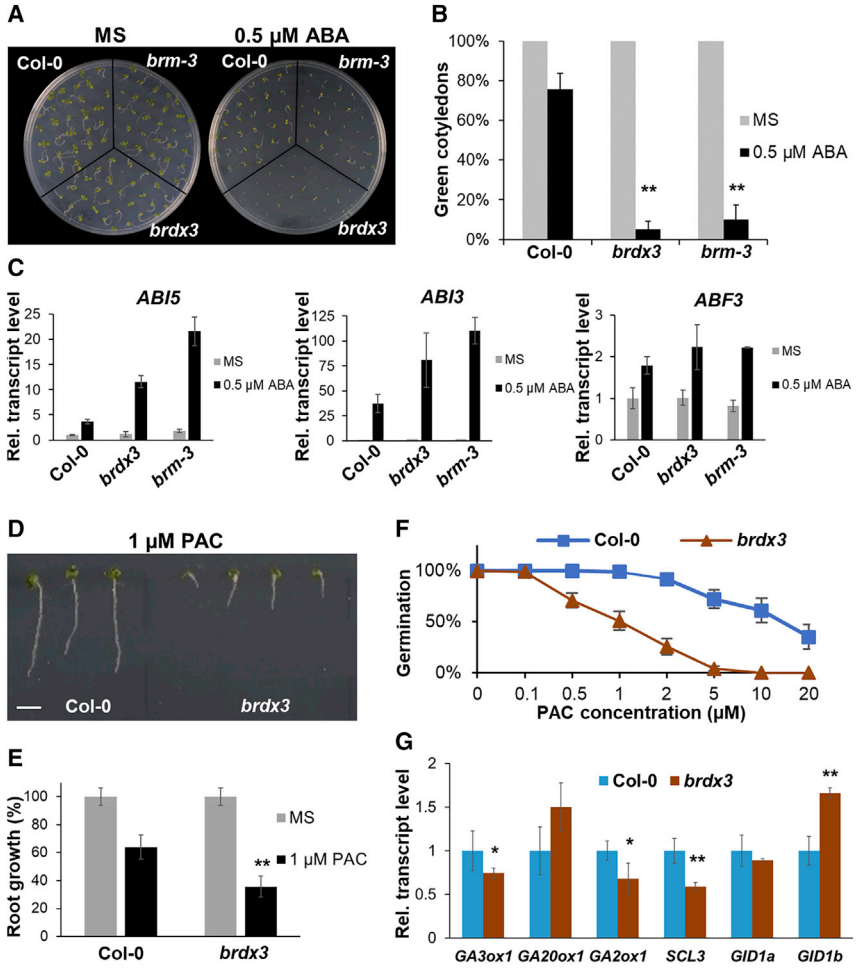

Figure 5. Hormonal responses of the *brdx3* mutant.

(A) The *brdx3* mutant shows hypersensitivity to ABA.

(B) The percentage of germinated embryos developing green cotyledons in the presence of 0.5 μM ABA. Values are the mean ± STD. Asterisks indicate significant differences from the WT (χ^2 test, $n = 105$, $P < 10^{-11}$).

(C) RT-qPCR analysis of ABA pathway transcriptional regulator expression in 7-day-old WT, *brdx3*, and *brm-3* plants grown on MS or 0.5 μM ABA. The housekeeping gene *PP2A* was used as the normalization control. Means ± STD from three biological replicates are shown. Transcript levels in the WT are set to 1.

(D) Roots of WT and *brdx3* plants grown for 10 days on medium containing 1 μM PAC. Scale bar, 10 mm.

(E) Root growth inhibition in *brdx3* plants caused by PAC. Asterisks indicate significant differences from the WT plants (Student's *t*-test, $n = 30$, $P < 0.001$).

(F) Germination assay of the WT Col-0 and *brdx3* mutant in the presence of different concentrations of PAC. Radicle emergence after 12 days was scored as germination. Values are the mean ± STD.

(G) RT-qPCR analysis of GA pathway gene expression in 15-day-old WT and *brdx3* plants grown in soil under LD conditions. The housekeeping gene *PP2A* was used as the normalization control. Means ± STD from three biological replicates are shown. Transcript levels in the WT are set to 1. Asterisks indicate significant differences from the WT plants (Student's *t*-test, $^*P < 0.05$, $^{**}P < 0.01$).

genes previously shown to be controlled by the SWI/SNF complex. Compared with the WT, the expression of *ABI5* and *ABI3*, key transcriptional regulators in the ABA pathway (Cutler et al., 2010) that are controlled directly by BRM (Han et al., 2012), were moderately upregulated in 7-day-old seedlings of *brdx3* and *brm-3* grown on Murashige and Skoog (MS) medium (Figure 5C). These differences were significantly greater when seedlings were grown in the presence of ABA. *ABI5* was about 10-fold upregulated in *brdx3* and *brm-3*, compared with approximately 3.5-fold upregulation in the WT. Likewise, *ABI3* was upregulated by 48- and 62-fold in *brdx3* and *brm-3*, respectively, compared with 37-fold upregulation in the WT (Figure 5C). The differences between the two mutants and the WT in response to ABA treatment were even greater in older seedlings (supplemental Figure 13). By contrast, the transcript level of *ABF3*, which encodes an ABA pathway transcription factor that is not a BRM target in seedlings (Han et al., 2012), was not significantly changed (Figure 5C and supplemental Figure 13). Together, these results indicate that, similar to major SWI/SNF core subunits, BRDs regulate ABA responses primarily through the repression of *ABI3* and *ABI5*.

PAC treatment of *brdx3* mutants caused increased retardation of root growth (Figure 5D and 5E) and reduced seed germination (Figure 5F) relative to WT plants that received the same treatment. While not as strong as that of *brdx3*, PAC hypersensitivity was also observed in the *brd* single mutants (supplemental Figure 12B). RT-qPCR analysis of *brdx3* seedlings grown under normal conditions demonstrated that expression of the GA metabolism genes *GA3ox1* and *GA2ox1* and the GA pathway-related gene *SCL3* was downregulated relative to the WT, whereas expression of the GA receptor *GID1b* was upregulated (Figure 5G). Importantly, the PAC-induced phenotypes and transcriptional changes in *brdx3* were similar to those reported in *brm* mutants (Archacki et al., 2013). The similar phenotypic changes and mis-expression of ABA- and GA-responsive genes in *brdx3* and *brm-3* mutants indicate that BRD subunits are important players in SWI/SNF-mediated regulation of ABA and GA responses.

BRD depletion affects BRM protein levels and BRM binding to *SCL3*, *ABI5*, and *SVP* target genes

We next wanted to check whether the elimination of BRD subunits would affect the binding of BRM to selected direct target genes: *SCL3*, *ABI5*, and *SVP*. To this end, we constructed an *Arabidopsis* line that expressed BRM-GFP in the *brdx3 brm-1* mutant background. The BRM-GFP signal was reduced in this line compared with *brm-1*/BRM-GFP (Figure 6A and 6B). To corroborate this finding, we measured *BRM* mRNA and native BRM protein levels in the *brdx3* mutant. Compared with the WT, levels of the *BRM* transcript were slightly increased in *brdx3*, whereas the amount of BRM protein was reduced

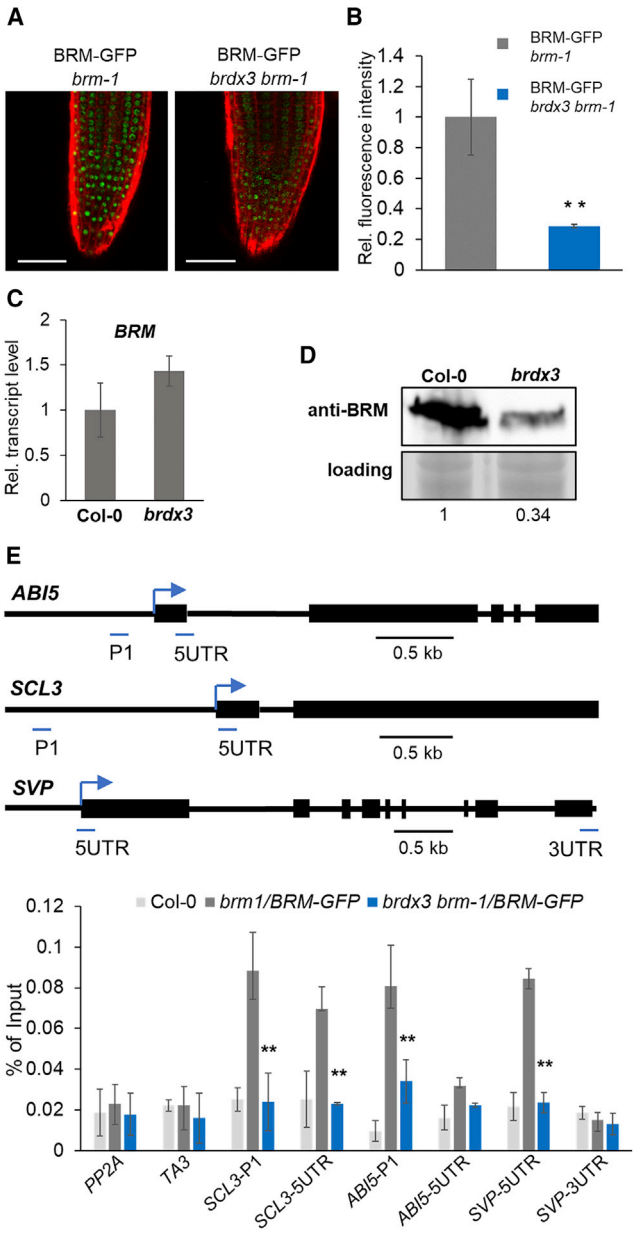

Figure 6. The *brdx3* mutation affects BRM protein levels and the binding of BRM to *SCL3*, *ABI5*, and *SVP* target genes.

(A) Confocal microscope images of root tips of *brm-1* and *brdx3 brm-1* mutants expressing BRM-GFP. Propidium iodide was used to counterstain cell walls. Scale bars, 50 μm.

(B) Relative fluorescence intensity of BRM-GFP in the roots of *brm-1* and *brdx3 brm-1* mutants. Values are mean ± STD from 10 measurements of each line. Asterisks indicate a significant difference between *brm-1/BRM-GFP* and *brdx3 brm-1/BRM-GFP* (Student's *t*-test, $P < 0.001$).

(C) RT-qPCR analysis of *BRM* transcript levels in the WT and *brdx3* mutant. The housekeeping gene *PP2A* was used as the normalization control. Means ± STD from three biological replicates are shown. The transcript level in the WT is set to 1.

(D) Western blot analysis of native BRM protein in 7-day-old WT and *brdx3* mutant plants. Signal intensities normalized to the loading control (Coomassie-stained gel) are shown by numbers beneath the figure.

(E) BRM enrichment at *SCL3*, *ABI5*, and *SVP* loci analyzed by ChIP–qPCR in 7-day-old *brm-1/BRM-GFP* and *brdx3 brm-1/BRM-GFP* plants. Means ± STD from three biological replicates are shown. *PP2A* and *TA3* sequences served as negative controls. Schematic diagrams of the tested loci and amplified regions are shown in the upper panel. Asterisks indicate significant differences between *brm-1/BRM-GFP* and *brdx3 brm-1/BRM-GFP* (Student's *t*-test, $P < 0.01$).

(Figure 6C and 6D), indicating that BRM is negatively regulated at the protein level in the absence of BRDs. Chromatin immunoprecipitation (ChIP) assays clearly showed enrichment of BRM-GFP in the *SCL3*, *ABI5*, and *SVP* promoter regions, consistent with previous reports (Han et al., 2012; Archacki et al., 2013, 2017; Li et al., 2015). However, the occupancy of BRM at these targets was strongly reduced in the *brdx3* mutant (Figure 6E). This may be due either to the decreased level of BRM-GFP in *brdx3* (resulting in fewer precipitated DNA–BRM complexes), or to impaired targeting of the SWI/SNF complex to these loci in the absence of BRD subunits, or both.

The *bromo4* mutation abolishes SWI/SNF function

To determine the effect of eliminating all known bromodomains located in the *Arabidopsis* SWI/SNF complex, we combined the *brm-3* hypomorphic mutant (Farrona et al., 2007), which expresses a truncated BRM ATPase lacking the bromodomain (Figure 7A), with *brdx3* to construct a quadruple *brm-3 brd1 brd2 brd13* (*bromo4*) line. The truncated BRM protein was present in the nuclear extract of *bromo4*, although its level was decreased compared with that in *brm-3*, similar to the reduction in the level of full-length BRM in the *brdx3* mutant compared with the WT (Figure 7B). Remarkably, *bromo4* plants displayed a strong phenotype that phenocopied the *brm-1* null mutant in which the BRM-containing SWI/SNF complex is non-functional. This phenotype consists of short roots (supplemental Figure 14), greatly reduced rosette size, enhanced leaf curling (Figure 7C and 7D), frequent and severe floral organ defects (Figure 7E and supplemental Table 2), and complete sterility (Figure 7F). Leaf curling is one of the most characteristic traits of SWI/SNF core subunit mutants such as *brm*, *swi3c*, and *swp73b* (Hurtado et al., 2006; Sacharowski et al., 2015; Sarnowski et al., 2005). In these mutants, the leaf blade is twisted along the proximal–distal axis and curved downward toward the abaxial surface. We observed that this leaf phenotype is strengthened as the number of bromodomains in the SWI/SNF complex decreases (Figure 7G). Leaf curling is only slight in *brm-3*, more pronounced in *brdx3*, and most severe in *bromo4*, whose leaves have the same morphology as those of the *brm-1* null mutant (Figure 7F and 7G). Interestingly, almost the same changes were present in the leaves of a heterozygous *bromo4* mutant (*brm-3*$^{-/+}$ *brd1*$^{-/-}$ *brd2*$^{-/-}$ *brd13*$^{-/-}$), suggesting a dosage-dependent effect of bromodomain depletion (supplemental Figure 15). In *Arabidopsis*, the adaxial identity of cells is promoted by the class III homeodomain-leucine zipper (HD-ZIP)-encoding genes PHAVOLUTA (PHV), PHABULOSA (PHB), and REVOLUTA (REV), whereas abaxial identity is promoted by the KANADI (KAN) and YABBY (YAB) gene families (Du et al., 2018). In addition, two genes encoding auxin-responsive factors, ARF3 and ARF4, are also involved in abaxial specification. We therefore investigated the expression levels of key genes controlling leaf polarity in the bromodomain-depleted mutants and in *brm-1* (Figure 7H). RT-qPCR analysis showed that most of the genes involved in abaxial cell fate (*ARF3*, *FIL (YAB1)*, *YAB3*, *YAB5*,

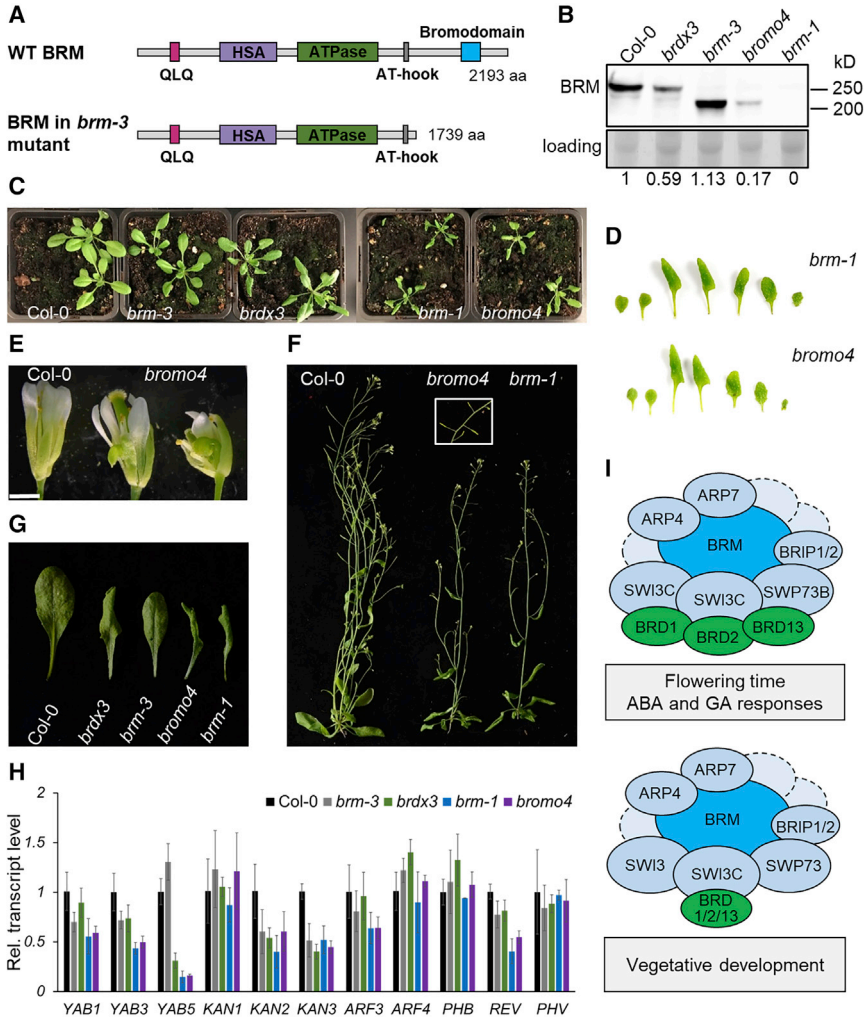

Figure 7. *Bromo4* is a phenocopy of the *brm-1* null mutant.

(A) Expression of the truncated BRM ATPase lacking the C-terminal region encompassing the bromodomain in the *brm-3* mutant.

(B) Western blot analysis of native BRM protein in 3-week-old WT and mutant plants. Signal intensities normalized to the loading control are shown by numbers beneath the figure.

(C) Rosette phenotypes of the analyzed mutants.

(D) Leaf series of *bromo4* and *brm-1* mutants.

(E) A WT flower and two highly aberrant flowers of the *bromo4* mutant.

(F) Adult plants of the WT and *bromo4* mutant. The inset shows the shortened sterile siliques of *bromo4*.

(G) Leaf morphology of the analyzed mutants.

(H) qRT–PCR analysis of the transcript levels of genes involved in the determination of leaf polarity. RT-qPCR was performed using total RNA isolated from 18-day-old rosette leaves. The housekeeping gene *PP2A* was used as the normalization control. Transcript levels in the WT are set to 1. Error bars indicate the STD of three independent biological replicates.

(I) Model of the functions of BRDs as subunits of *Arabidopsis* SWI/SNF complexes. The two SWI/SNF complexes shown contain either one or multiple BRD proteins. Only subunits confirmed to co-purify with BRM ATPase are shown, and the putative uncharacterized subunits are depicted with dashed circles.

and *KAN2*) and one gene involved in adaxial cell fate (*REV*) were downregulated in the analyzed mutants relative to WT plants. Transcript levels of the *YAB* genes, *ARF3*, and *REV* showed moderate changes in *brm-3* and *brdx3*; they decreased further and attained very similar levels in the *bromo4* and *brm-1* mutants (Figure 7H). This result is consistent with the observed leaf phenotypes, indicating that loss of the three BRD proteins and BRM bromodomain is functionally equivalent to the removal of the SWI/SNF catalytic subunit BRM.

DISCUSSION

The occurrence of bromodomain-containing proteins in plant SWI/SNF complexes was postulated previously (Jerzmanowski, 2007), and this hypothesis gained support with the demonstration in *Arabidopsis* and maize that several BRD proteins could be co-precipitated with major subunits of SWI/SNF complexes (Vercruyssen et al., 2014; Nelissen et al., 2015). Nonetheless, until now there have been no data indicating how these putative components of SWI/SNF remodelers are related to other plant, yeast, or animal bromodomain-containing proteins, how they bind to the complexes, and what their physiological significance is in plants. In this study, we have established that BRD1, BRD2, and BRD13 are likely bona fide components of *Arabidopsis* SWI/SNF complexes. The relatively minor phenotypic changes between WT plants and single-gene *BRD* mutants and the lack of substantial differences among single *BRD* mutants and between single and double mutants indicate that BRD proteins in SWI/SNF complexes are individually non-essential and functionally redundant. Depletion of all three proteins produced a stronger phenotype that resembled that of mutants in the major SWI/SNF subunits BRM and SWI3C. We obtained a quadruple mutant by depletion of the three BRD proteins in a hypomorphic BRM mutant line whose BRM ATPase lacked the bromodomain motif. Significantly, this mutant phenocopied null BRM mutants, providing strong genetic evidence that BRDs and BRM act as components of the same complexes and that there is cooperation between BRD subunits and the bromodomain of the BRM ATPase.

Implications for SWI/SNF composition in *Arabidopsis*

According to recent reports, yeast SWI/SNF remodelers contain one (ySWI/SNF) or six (RSC) bromodomains (Ye et al., 2019), whereas mammalian complexes carry one (cBAF), two (ncBAF), or multiple bromodomains (eight or more in PBAF) (Mashtalir et al., 2018). In addition to tandemly arranged bromodomains, yeast RSC1 and RSC2 and animal Polybromo subunits of PBAF-type SWI/SNF complexes all contain a bromo-adjacent homology domain that binds histone H3 (Chambers et al., 2013). No such module occurs in *Arabidopsis* BRD1, BRD2, or BRD13, consistent with its absence in the closely related mammalian

BRD7 and BRD9 proteins (Figure 1B). Together with the absence of proteins with multiple bromodomains in *Arabidopsis*, this suggests that the split into BAF- and PBAF-like SWI/SNF chromatin remodelers, evolutionarily conserved in yeast and animals, did not occur or has not been preserved in plants. Instead, our findings corroborate an earlier hypothesis that the functions of PBAF-like remodelers can be fulfilled in plants by complexes that contain several auxiliary subunits, each with a single bromodomain (Jerzmanowski, 2007). We showed that the core SWI/SNF subunits SWI3C and SWP73B are capable of direct protein-protein interactions with each of the three *Arabidopsis* BRD proteins (Figures 2 and 3). These two subunits could therefore mediate simultaneous binding of pair-wise combinations of the three BRD proteins to SWI/SNF complexes while retaining the ability to interact with each other (supplemental Figure 3). Given that each SWI/SNF complex contains two copies of the SWI3 subunit (Han et al., 2020; He et al., 2020; Sarnowski et al., 2005), complexes containing three BRD proteins are likely to be present in *Arabidopsis*. In agreement with this assumption, SWI3C, SWP73B, and all three BRDs were found among proteins that co-precipitated with BRM-GFP in IP/MS experiments (Figure 1A and supplemental Table 1). However, our previous demonstration that BRDs were absent among SWI/SNF subunits that co-purified with GFP-tagged histone deacetylase HD2C (Buszewicz et al., 2016) indicates that SWI/SNF complexes lacking BRD subunits may also exist. Such complexes would still retain the one bromodomain that occurs in the BRM ATPase, similar to yeast SWI/SNF and mammalian cBAF remodelers (Mashtalir et al., 2018; Han et al., 2020). Indeed, among the four-member family of *Arabidopsis* SWI3 subunit variants (SWI3A–D) and the two-member SWP73 subunit family (SWP73A–B), only SWI3C and SWP73B were capable of BRD binding, indicating that the number of BRD copies per complex will depend on the SWI3 and SWP73 isoforms present. Thus, a spectrum of SWI/SNF complexes with different subunit compositions is possible, ranging from those without BRDs (in complexes with SWP73A and SWI3A/B/D as core subunits) to those with three BRDs (in complexes with SWP73B and two copies of SWI3C). Because not all *Arabidopsis* SWI/SNF subunits have been characterized to date and could be tested for interactions in our assays, we do not rule out the possibility that additional copies of BRD proteins may be incorporated into the complex. The exact number and identity of BRDs in *Arabidopsis* SWI/SNF assemblies may only be established upon the development of improved biochemical and proteomic methods for the isolation and purification of homogenous complexes, as demonstrated recently for mammalian SWI/SNF remodelers (Mashtalir et al., 2018).

Redundant roles of BRDs in *Arabidopsis* development and hormonal responses

Comparison of the phenotypic effects of null mutations in single genes encoding *Arabidopsis* BRD proteins showed that BRD1, BRD2, and BRD13 are mostly functionally redundant. The absence of any one of the three BRD proteins had no visible impact on the growth or appearance of mutants in the vegetative phase compared with that of WT plants (except for a small difference in third and fourth leaf curvature in *brd13* mutants), but moderately accelerated flowering was observed. Changes in flowering time were additive in double *brd* mutants, and these were consistent with gene expression data that showed significant increases in the expression of *FT* and *FUL*, two key genes involved in the regulation of flowering (Figure 4K and supplemental Figure 10). Moreover, *brdx3* mutants showed changes in transcript levels of the flowering repressors *FLC* and *SVP* (supplemental Figure 10C), similar to those demonstrated previously in *brm-1* (Farrona et al., 2011; Li et al., 2015). The FLC-SVP complex is known to bind and repress *FT* (Mateos et al., 2015), and it was therefore proposed that, despite increased *FLC* expression, the downregulation of *SVP* could explain *FT* upregulation and the early flowering phenotype of *brm* mutants (Li et al., 2015). Similarly, the decrease in BRM binding to the *SVP* promoter (Figure 6E) and the downregulation of *SVP* expression observed in the *brdx3* mutant could be at least partly responsible for *FT* upregulation in this mutant. However, this hypothesis remains to be verified experimentally. With regard to the roles of BRDs in other developmental pathways, the similarity of the effects observed in single and double mutants demonstrated that each of the three BRD subunits could mostly compensate for a lack of the other two. This result is consistent with the almost identical spatio-temporal profiles of the transcriptional activity of their respective genes (supplemental Figure 7). The minimal differences in functional effects among these mutants suggest that the individual roles of particular BRD proteins are likely to be narrow and subtle, probably affecting fitness only under highly specific environmental conditions. The overall significance of BRD subunits could be seen in plants depleted of all three. Compared with single and double *brd* mutants, *brdx3* plants showed a considerably greater number of mis-regulated genes (Figure 4L and supplemental Data 2), consistent with their numerous defects in vegetative development and flowering. Importantly, the phenotypic and gene expression changes observed in *brdx3* plants, including defects in ABA and GA responses, resembled those seen in mutants of genes encoding the BRM or SWI3C subunits of the SWI/SNF complex (Figures 4G–4I and 5), indicating that BRDs, BRM, and SWI3C act in a common complex. This was further confirmed by the non-additive phenotype of the *brm-1 brdx3* quadruple mutant (supplemental Figure 8) and fits with the upregulation of *BRD* genes in *brm-1*, most likely through a compensatory feedback mechanism (supplemental Figure 9). It is also supported by global gene expression analyses that showed considerable overlap between the *brdx3* and *brm-1* mutants, as well as similar GO categories enriched in *brdx3* plants and in mutants that lack major SWI/SNF subunits, including BRM and SWP73B (Sacharowski et al., 2015; Archacki et al., 2017) (Figure 4M). Interestingly, the ABA- and GA-related phenotypes could be detected in single *brd* mutants (supplemental Figure 12) simultaneously with the defective flowering phenotype. This may be explained by the different subunit composition of SWI/SNF complexes required for the regulation of flowering and hormonal responses, as opposed to those involved in other developmental processes, such as leaf polarity specification. Thus, flowering and hormonal responses would be mediated by complexes containing three different BRDs, whereas the control of leaf development would require complexes containing only one (BRD1, BRD2, or BRD13) or two BRDs (Figure 7I). This scenario would explain why BRDs can compensate for each other in most but not all functions.

Importance of BRDs and bromodomains for SWI/SNF functions

The importance of BRD subunits for SWI/SNF functions was demonstrated by showing that the binding of BRM ATPase to its direct target genes *SCL3*, *ABI5*, and *SVP* was strongly affected in the *brdx3* mutant (Figure 6E). This may reflect impaired recruitment of the SWI/SNF complex, reduction of BRM protein levels in the absence of *BRD* subunits, or both. Further experiments are required to uncouple these two possible functions of BRDs and determine their role in SWI/SNF binding to chromatin. The negative effect of BRD depletion on BRM protein levels (Figures 6A–6D and 7B) is rather surprising, as BRDs represent auxiliary subunits and in mammals do not seem to have an impact on the level of the core subunits (including the ATPase) (Mashtalir et al., 2018). However, reduced levels of the BRM protein have also recently been reported in an *Arabidopsis brip1/2* mutant that lacks homologs of mammalian glioma tumor-suppressor candidate region domain-containing subunits (Yu et al., 2020). Together, these data suggest that the stabilization of SWI/SNF complexes in *Arabidopsis* may require assembly of the full complement of subunits. The most direct indication of the role of BRD subunits in SWI/SNF complexes is provided by the observation that a quadruple *bromo4* mutant deprived of all three BRDs and the bromodomain of the BRM ATPase exactly phenocopied the *brm-1* mutant, which lacks BRM ATPase completely. This resemblance was apparent at both the morphological and molecular levels (Figure 7C–7H). Importantly, the effects of removing the full set of bromodomains were dosage-dependent, with *bromo4* heterozygotes displaying a phenotype intermediate between those of *bromo4* and *brdx3* homozygotes (supplemental Figure 15). One interpretation of these results is that the depletion of all bromodomains from the SWI/SNF complex is the major cause of the strong null-like phenotype. In such a scenario, mutation of BRD subunits or deprivation of BRM ATPase of its bromodomain both lead to the formation of mostly active SWI/SNF complexes that retain many of their functions, as demonstrated by the relatively mild phenotypes of *brm-3* and *brdx3* mutants. It is only the loss of all bromodomains from the SWI/SNF complex that reveals their critical importance. Alternatively, the lower level of truncated BRM in *bromo4* (Figure 7B) may no longer provide sufficient SWI/SNF activity. It remains to be determined whether the bromodomains of *Arabidopsis* SWI/SNF chromatin remodelers act *in vivo* primarily by targeting these complexes to acetylated nucleosomes or by exerting other modulatory effects on SWI/SNF activity.

METHODS

Plant lines and growth conditions

Arabidopsis thaliana WT and all mutant lines were of the Columbia-0 (Col-0) ecotype. The *brm-1* and *brm-3* mutants have been characterized previously (Hurtado et al., 2006; Farrona et al., 2007). Insertion mutants in *BRD* genes were obtained from the Nottingham Arabidopsis Stock Centre. Five *BRD1* mutations, two *BRD2* mutations, and four *BRD13* mutations were initially tested: *brd1-1* (SALK_049806), *brd1-2* (SALK_012963), *brd1-3* (SALK_046437), *brd1-4* (GK-085D08), *brd1-5* (GK-219B04), *brd2-1* (SALK_025965), *brd2-2* (SALK_004343), *brd13-1* (SALK_10 216), *brd13-2* (SAIL_557_E12), *brd13-3* (GK-717A09), and *brd13-4* (SALK_208635C). Two mutant alleles for each *BRD* gene were subsequently selected for further analyses based on their phenotypes and the expression levels of the mutated genes. The locations of T-DNA insertions were confirmed by sequencing allele-specific PCR products. The *pBRM*:*BRM-GFP* transgenic line was kindly provided by Dr. K. Kaufmann (Smaczniak et al., 2012). The *brm-1/BRM-GFP* and *brdx3 brm-1/BRM-GFP* lines were constructed by crossing the *pBRM*:*BRM-GFP* line with the respective mutants. Homozygous lines were identified by genotyping. *brm-1 brdx3* mutants were identified from segregating progeny of the *brdx3 brm-1/BRM-GFP*$^{+/-}$ line. Primers used for mutant genotyping are listed in supplemental Table 3.

For all experiments, seeds were surface sterilized with gaseous chlorine for 3–5 h and stratified for 2–3 days at 4°C. Seeds were sown on a mixture of soil and vermiculite (3:1) or plated on half-strength MS medium containing 0.5% sucrose and 0.8% agar. Plants were grown under LD (16 h light/8 h dark) or SD (8 h light/16 h dark) conditions at 22°C/19°C. Flowering time was scored as the number of days after stratification (DAS). The number of rosette leaves and days to flowering were counted after the main stem had bolted by 1 cm. For IP/MS analysis, seedlings were grown in liquid $^1/_2$ MS medium supplemented with $^1/_2$ MS vitamin solution (43 mg/l Fe-Na-EDTA, 100 mg/l myo-inositol, 500 mg/l MES) and 0.5% sucrose, as described previously (Kulik et al., 2012).

Physiological assays

For the germination assay, seeds were sown on MS plates supplemented with different concentrations of PAC. To score seed germination rate, plants were counted at 7 DAS. Seeds that did not show radicle emergence were scored as not germinated. For seedling growth (green cotyledon) assays, seeds were sown on MS plates supplemented with ABA at a concentration of 0.5 or 1 μM. Plants that had formed green cotyledons were counted at 7 DAS.

Y2H assays

Plasmid vectors pGAD424 and pGBT9 (Clontech) containing the cDNAs of *BRM*, *SWI3A*, *SWI3B*, *BSH*, and *SWP73B* were described previously (Buszewicz et al., 2016). The full-length cDNAs of *BRD1*, *BRD2*, *BRD13*, *SWI3C*, *SWI3D*, *SWP73A*, *ARP4*, and *ARP7* and a cDNA encoding the N-terminal region of SYD (1–1500 bp of the coding sequence) were cloned into pGAD424 and pGBT9 by ligation with T4 DNA ligase (Thermo Scientific) or using the SLIC protocol (Li and Elledge, 2007). Cells of the yeast strain AH109 were transformed with plasmid DNA as described previously (Buszewicz et al., 2016). Serial 10-fold dilutions of the transformant cell suspensions were plated on synthetic dropout medium (Sigma) lacking tryptophan, leucine, and histidine without additions or supplemented with 3-amine-1,2,4-triazole (3-AT) at 0.25–1 mM. The growth of each strain was assessed after incubating the plates for 3 days at 28°C. Three technical replicates were performed for each strain in each growth assay.

Y3H assays

The Y2H system was modified by introducing a third plasmid expressing SWI3C, BRD1, or BRD13. To generate these constructs, the full-length coding sequence of each gene was PCR-amplified using primers encoding an SV40 NLS added to the N terminus to ensure nuclear localization in yeast cells (Sun et al., 2011) and cloned into the BamHI/SalI sites of the plasmid p426 carrying the URA3 nutritional marker to permit selection on uracil-deficient medium (Mumberg et al., 1995). Yeast strain PJ64-4A was co-transformed with the indicated combinations of plasmids (James et al., 1996), and transformants were selected on synthetic dropout medium (Sigma) lacking tryptophan, leucine, and uracil. Serial 10-fold dilutions of the transformant cell suspensions were plated onto synthetic dropout medium lacking tryptophan, leucine, uracil, and histidine (W0 medium) without additions or supplemented with 3-AT at concentrations of 1–10 mM. The growth of each strain was assessed after incubating the plates for 3–4 days at 28°C. Three technical replicates were performed for each strain in each growth assay.

BiFC and localization analyses

Full-length *BRD1*, *BRD2*, *BRD13*, and *SWI3C* cDNAs were cloned into the pDONR201 vector and verified by sequencing. Corresponding entry clones were used in LR recombination reactions to transfer the DNA fragments into the gateway-compatible expression vectors pYFN43 and pYFC43 for BiFC assays (Belda-Palazón et al., 2012) or the pGWB series vector pGWB605 (Nakamura et al., 2010) for localization analyses. The obtained binary constructs were used to transform *Agrobacterium tumefaciens* GV3101. Each pGWB605 construct or the combinations of YFPN and YFPC fusion constructs were co-expressed in 6- to 8-week-old *Nicotiana benthamiana* leaves after leaf infiltration with GV3101 strains containing the tested construct combinations plus an anti-silencing *Agrobacterium* strain expressing P19. In addition, an *Agrobacterium* strain transformed with 35S::H2B-RFP was used to visualize the nuclei. Fluorescence was analyzed 2 days after infiltration using a Nikon D-Eclipse C1 laser scanning confocal microscope.

RNA extraction, RT–PCR, and RT-qPCR analyses

The expression of flowering control genes was analyzed in the aerial parts of 15-day-old or 4-week-old seedlings grown in soil under LD or SD conditions, respectively. Plant material was collected ~3 h before the lights went off because *FT* expression is high at this time (Shim et al., 2017). Two-week-old seedlings from MS plates were used for RT-qPCR analyses after ABA treatment. RNA was extracted from plant material using a GeneJET RNA Purification Kit (Thermo Scientific) and then digested with TURBO DNase (Ambion). Total RNA (1 μg) was reverse-transcribed using a Transcriptor First-Strand cDNA Synthesis Kit (Roche). qPCR analyses were performed using SYBR Green I Master Mix in a LightCycler 96 (Roche) with gene-specific primers (supplemental Table 3). The transcript level of each gene was normalized to that of the housekeeping gene *PP2A*. Three biological replicates were examined for each genotype.

Microarray analysis

For microarray analysis, the aerial parts of 18-day-old WT, *brd2-1*, *brd1-2 brd2-1*, and *brd1-2 brd2-1 brd13-4* (*brdx3*) seedlings were collected in three biological replicates. RNA was extracted using an RNeasy Plant Kit (QIAGEN) and digested with TURBO DNase (Ambion). Microarray hybridization was performed as described previously (Buszewicz et al., 2016) using the Affymetrix Gene Atlas system according to the manufacturer's instructions. Data analysis was performed using Bioconductor packages in the R environment. Raw CEL files were annotated to the associated annotation package pd.aragene 1.1 st built with the pdInfoBuilder package (Falcon et al., 2020). Normalization of the raw intensities was performed using the Robust Multiarray Averaging method from the oligo package (Carvalho and Irizarry, 2010). Differential gene expression analysis was performed with the limma package (Ritchie et al., 2015). Data were fitted to a linear model, and moderated *t*-statistics were computed by empirical Bayes moderation. A gene was identified as differentially expressed in a selected genotype when the *P* value was <0.01 and the expression fold change was >1.5 relative to the WT. Overlap between *brdx3* and *brm-1* transcriptional profiles was analyzed using a published dataset (Buszewicz et al., 2016). Genes were selected as differentially expressed based on the same *P* value (<0.01) and fold change (>1.5) values. The AgriGO online tool was used for GO analysis (http://systemsbiology.cau.edu.cn/agriGOv2/) (Tian et al., 2017). Venn diagrams were constructed using the DeepVenn tool (Hulsen et al., 2008).

Western blotting

Native BRM protein was detected by western blotting as described previously (Archacki et al., 2017). The analyzed samples were whole-cell extracts for MS-grown seedlings and nuclear extracts for plants grown in soil. The relative BRM signal was quantified with ImageJ software by comparison with the protein level on the Coomassie-stained gel (loading control).

ChIP

Chromatin was isolated from MS-grown 7-day-old seedlings of the WT, *brm-1/BRM-GFP*, and *brdx3 brm-1/BRM-GFP* lines. ChIP was performed as described previously (Archacki et al., 2017) except that GFP-Trap (ChromoTek) was used to immunoprecipitate BRM-GFP. The extracted DNA was resuspended in 100 μl of water. ChIP enrichment was determined by qPCR using SYBR Green I Master mix in a LightCycler 96 (Roche) with gene-specific primers (supplemental Table 3). Reactions were performed with 1 μl of immunoprecipitated DNA as template. The amount of ChIP DNA was calculated based on the standard curve and relative to the input sample for each pair of primers. The *TA3* retrotransposon and *PP2A* coding sequence served as controls.

IP/MS

Nuclear proteins were extracted from 14-day-old plants according to ChromoTek's application note (https://resources.chromotek.com/an_gfp_immunoprecipitation_a-thaliana). In brief, 2 g of ground plant material was resuspended in lysis buffer (50 mM Tris–HCl [pH 7.5], 150 mM NaCl, 5 mM $MgCl_2$, 1% Triton X-100, 2% glycerol, 5 mM DTT, 1 mM PMSF) containing protease inhibitors (cOmplete EDTA-free, Roche), proteasome inhibitor MG132 (Sigma), and phosphatase inhibitors (PhosSTOP, Roche), as the BRM protein is susceptible to degradation and is phosphorylated *in vivo* (Peirats-Llobet et al., 2016). The cell lysates were centrifuged at 20 000 × *g* for 15 min at 4°C, and cleared supernatant was mixed with 25 μl of GFP-Trap agarose beads (ChromoTek). After 45 min at 4°C, the beads were washed two times with lysis buffer and three times with washing buffer (50 mM Tris–HCl [pH 7.5], 150 mM NaCl, 1% glycerol, 1 mM DTT). The immunoprecipitated proteins were then subjected to on-bead digestion and MS analysis at the Laboratory of Mass Spectrometry, Institute of Biochemistry and Biophysics PAS (Warsaw) using a nanoACQUITY UPLC System (Waters Corporation) coupled to an Orbitrap Elite and Q Exative MS (Thermo Fisher Scientific). Peptide analysis and identification were performed as described previously (Buszewicz et al., 2016).

Phylogenetic analysis

Full-length amino acid sequences of yeast and human SWI/SNF subunits containing bromodomains, *Arabidopsis* BRD1, BRD2, and BRD13, and other proteins representing previously described classes of *Arabidopsis* bromodomain-containing proteins (Rao et al., 2014) were used for multiple sequence alignment with ClustalW (supplemental Table 4) (Larkin et al., 2007). A neighbor-joining tree was constructed using MEGA7 software (Kumar et al., 2016), and bootstrap probability values were obtained from 1000 iterations. Bromodomains were detected using the ScanProsite tool from the Prosite database.

ACCESSION NUMBERS

Sequence data from this article can be found in The Arabidopsis Information Resource (TAIR) database under the following accession numbers: *BRD1* (AT1G20670), *BRD2* (AT1G76380), *BRD13* (AT5G55040), and *BRM* (AT2G46020). Microarray data are available in the ArrayExpress database (www.ebi.ac.uk/arrayexpress) under accession number E-MTAB-9688.

SUPPLEMENTAL INFORMATION

Supplemental information is available at *Plant Communications Online*.

FUNDING

This work was supported by grants from National Science Centre project nos. 2014/15/N/NZ2/00 396 to K.J., 2014/13/B/NZ1/00 967 to A.J., and 2017/26/E/NZ2/00 899 to R.A. The equipment used in the mass spectrometry laboratory was sponsored in part by the Center for Preclinical Research and Technology (CePT), a project co-sponsored by the European Regional Development Fund and Innovative Economy, The National Cohesion Strategy of Poland.

AUTHOR CONTRIBUTIONS

Conceptualization, K.J. and R.A.; investigation, K.J., K.S., A.Z., P.P., E.M., N.S., P.S., M.B., R.I.-W., and M.K.; writing – original draft, R.A.; writing – review & editing, R.A. and A.J.; funding acquisition, K.J., A.J., and R.A.; supervision, A.J and R.A.

ACKNOWLEDGMENTS

We would like to thank Dr. K. Kaufmann (Humboldt-Universitat zu Berlin) for providing the BRM-GFP transgenic line, M. Marczak for technical support, M. Lichocka for assisting with confocal microscopy, and D. Buszewicz and S. Swiezewski (IBB PAS) for comments on the manuscript. The authors acknowledge networking support from the "INDEPTH" COST Action CA16212. No conflict of interest declared.

Received: October 20, 2020
Revised: January 12, 2021
Accepted: March 2, 2021
Published: March 5, 2021

REFERENCES

Archacki, R., Buszewicz, D., Sarnowski, T.J., Sarnowska, E., Rolicka, A.T., Tohge, T., Fernie, A.R., Jikumaru, Y., Kotlinski, M., Iwanicka-Nowicka, R., et al. (2013). BRAHMA ATPase of the SWI/SNF chromatin remodeling complex acts as a positive regulator of gibberellin-mediated responses in *Arabidopsis*. PLoS One **8**:e58588.

Archacki, R., Yatusevich, R., Buszewicz, D., Krzyczmonik, K., Patryn, J., Iwanicka-Nowicka, R., Biecek, P., Wilczynski, B., Koblowska, M., Jerzmanowski, A., et al. (2017). *Arabidopsis* SWI/SNF chromatin remodeling complex binds both promoters and terminators to regulate gene expression. Nucleic Acids Res. **45**:3116–3129.

Awad, S., and Hassan, A.H. (2008). The Swi2/Snf2 bromodomain is important for the full binding and remodeling activity of the SWI/SNF complex on H3- and H4-acetylated nucleosomes. Ann. N. Y. Acad. Sci. **1138**:366–375.

Belda-Palazón, B., Ruiz, L., Martí, E., Tárraga, S., Tiburcio, A.F., Culiáñez, F., Farràs, R., Carrasco, P., and Ferrando, A. (2012). Aminopropyltransferases involved in polyamine biosynthesis localize preferentially in the nucleus of plant cells. PLoS One **7**:e46907.

Bezhani, S., Winter, C., Hershman, S., Wagner, J.D., Kennedy, J.F., Kwon, C.S., Pfluger, J., Su, Y., and Wagner, D. (2007). Unique, shared, and redundant roles for the *Arabidopsis* SWI/SNF chromatin remodeling ATPases BRAHMA and SPLAYED. Plant Cell **19**:403–416.

Buszewicz, D., Archacki, R., Palusiński, A., Kotliński, M., Fogtman, A., Iwanicka-Nowicka, R., Sosnowska, K., Kuciński, J., Pupel, P., Olędzki, J., et al. (2016). HD2C histone deacetylase and a SWI/SNF chromatin remodelling complex interact and both are involved in mediating the heat stress response in *Arabidopsis*. Plant Cell Environ. **39**:2108–2122.

Carvalho, B.S., and Irizarry, R.A. (2010). A framework for oligonucleotide microarray preprocessing. Bioinforma. Oxf. Engl. **26**:2363–2367.

Chambers, A.L., Pearl, L.H., Oliver, A.W., and Downs, J.A. (2013). The BAH domain of Rsc2 is a histone H3 binding domain. Nucleic Acids Res. **41**:9168–9182.

Chandrasekaran, R., and Thompson, M. (2007). Polybromo-1-bromodomains bind histone H3 at specific acetyl-lysine positions. Biochem. Biophys. Res. Commun. **355**:661–666.

Clapier, C.R., and Cairns, B.R. (2009). The biology of chromatin remodeling complexes. Annu. Rev. Biochem. **78**:273–304.

Cutler, S.R., Rodriguez, P.L., Finkelstein, R.R., and Abrams, S.R. (2010). Abscisic acid: emergence of a core signaling network. Annu. Rev. Plant Biol. **61**:651–679.

Du, F., Guan, C., and Jiao, Y. (2018). Molecular mechanisms of leaf morphogenesis. Mol. Plant **11**:1117–1134.

Elfring, L.K., Daniel, C., Papoulas, O., Deuring, R., Sarte, M., Moseley, S., Beek, S.J., Waldrip, W.R., Daubresse, G., DePace, A., et al. (1998). Genetic analysis of brahma: the *Drosophila* homolog of the yeast chromatin remodeling factor SWI2/SNF2. Genetics **148**:251–265.

Falcon, S., Carey, V., Settles, M., de Beuf, K., and Carvalho, B. (2020). pdInfoBuilder: Platform Design Information Package Builder. R Package Version 1.52.0.

Farrona, S., Hurtado, L., and Reyes, J.C. (2007). A nucleosome interaction module is required for normal function of *Arabidopsis thaliana* BRAHMA. J. Mol. Biol. **373**:240–250.

Farrona, S., Hurtado, L., March-Díaz, R., Schmitz, R.J., Florencio, F.J., Turck, F., Amasino, R.M., and Reyes, J.C. (2011). Brahma is required for proper expression of the floral repressor FLC in *Arabidopsis*. PLoS One **6**:e17997.

Filippakopoulos, P., Picaud, S., Mangos, M., Keates, T., Lambert, J.-P., Barsyte-Lovejoy, D., Felletar, I., Volkmer, R., Müller, S., Pawson, T., et al. (2012). Histone recognition and large-scale structural analysis of the human bromodomain family. Cell **149**:214–231.

Han, S.-K., Sang, Y., Rodrigues, A., BIOL425, F.2010, Wu, M.-F., Rodriguez, P.L., and Wagner, D. (2012). The SWI2/SNF2 chromatin remodeling ATPase BRAHMA represses abscisic acid responses in the absence of the stress stimulus in *Arabidopsis*. Plant Cell **24**:4892–4906.

Han, S.-K., Wu, M.-F., Cui, S., and Wagner, D. (2015). Roles and activities of chromatin remodeling ATPases in plants. Plant J. Cell Mol. Biol. **83**:62–77.

Han, Y., Reyes, A.A., Malik, S., and He, Y. (2020). Cryo-EM structure of SWI/SNF complex bound to a nucleosome. Nature **579**:452–455.

He, S., Wu, Z., Tian, Y., Yu, Z., Yu, J., Wang, X., Li, J., Liu, B., and Xu, Y. (2020). Structure of nucleosome-bound human BAF complex. Science **367**:875–881.

Ho, P.J., Lloyd, S.M., and Bao, X. (2019). Unwinding chromatin at the right places: how BAF is targeted to specific genomic locations during development. Dev. Camb. Engl. **146**. https://doi.org/10.1242/dev.178780.

Hohmann, A.F., Martin, L.J., Minder, J.L., Roe, J.-S., Shi, J., Steurer, S., Bader, G., McConnell, D., Pearson, M., Gerstberger, T., et al. (2016). Sensitivity and engineered resistance of myeloid leukemia cells to BRD9 inhibition. Nat. Chem. Biol. **12**:672–679.

Hulsen, T., de Vlieg, J., and Alkema, W. (2008). BioVenn—a web application for the comparison and visualization of biological lists using area-proportional Venn diagrams. BMC Genomics **9**:488.

Hurtado, L., Farrona, S., and Reyes, J.C. (2006). The putative SWI/SNF complex subunit BRAHMA activates flower homeotic genes in *Arabidopsis thaliana*. Plant Mol. Biol. **62**:291–304.

James, P., Halladay, J., and Craig, E.A. (1996). Genomic libraries and a host strain designed for highly efficient two-hybrid selection in yeast. Genetics **144**:1425–1436.

Jerzmanowski, A. (2007). SWI/SNF chromatin remodeling and linker histones in plants. Biochim. Biophys. Acta **1769**:330–345.

Kadoch, C., and Crabtree, G.R. (2015). Mammalian SWI/SNF chromatin remodeling complexes and cancer: mechanistic insights gained from human genomics. Sci. Adv. **1**:e1500447.

Knizewski, L., Ginalski, K., and Jerzmanowski, A. (2008). Snf2 proteins in plants: gene silencing and beyond. Trends Plant Sci. **13**:557–565.

Kulik, A., Anielska-Mazur, A., Bucholc, M., Koen, E., Szymanska, K., Zmienko, A., Krzywinska, E., Wawer, I., McLoughlin, F.,

Ruszkowski, D., et al. (2012). SNF1-related protein kinases type 2 are involved in plant responses to cadmium stress. Plant Physiol. **160**:868–883.

Kumar, S., Stecher, G., and Tamura, K. (2016). MEGA7: molecular evolutionary genetics analysis version 7.0 for bigger datasets. Mol. Biol. Evol. **33**:1870–1874.

Larkin, M.A., Blackshields, G., Brown, N.P., Chenna, R., McGettigan, P.A., McWilliam, H., Valentin, F., Wallace, I.M., Wilm, A., Lopez, R., et al. (2007). Clustal W and Clustal X version 2.0. Bioinformatics **23**:2947–2948.

Li, M.Z., and Elledge, S.J. (2007). Harnessing homologous recombination in vitro to generate recombinant DNA via SLIC. Nat. Methods **4**:251–256.

Li, C., Chen, C., Gao, L., Yang, S., Nguyen, V., Shi, X., Siminovitch, K., Kohalmi, S.E., Huang, S., Wu, K., et al. (2015). The *Arabidopsis* SWI2/SNF2 chromatin remodeler BRAHMA regulates polycomb function during vegetative development and directly activates the flowering repressor gene SVP. PLoS Genet. **11**:e1004944.

Mashtalir, N., D'Avino, A.R., Michel, B.C., Luo, J., Pan, J., Otto, J.E., Zullow, H.J., McKenzie, Z.M., Kubiak, R.L., St Pierre, R., et al. (2018). Modular organization and assembly of SWI/SNF family chromatin remodeling complexes. Cell **175**:1272–1288.e20.

Mateos, J.L., Madrigal, P., Tsuda, K., Rawat, V., Richter, R., Romera-Branchat, M., Fornara, F., Schneeberger, K., Krajewski, P., and Coupland, G. (2015). Combinatorial activities of SHORT VEGETATIVE PHASE and FLOWERING LOCUS C define distinct modes of flowering regulation in *Arabidopsis*. Genome Biol. **16**:31.

Morrison, E.A., Sanchez, J.C., Ronan, J.L., Farrell, D.P., Varzavand, K., Johnson, J.K., Gu, B.X., Crabtree, G.R., and Musselman, C.A. (2017). DNA binding drives the association of BRG1/hBRM bromodomains with nucleosomes. Nat. Commun. **8**:16080.

Mumberg, D., Müller, R., and Funk, M. (1995). Yeast vectors for the controlled expression of heterologous proteins in different genetic backgrounds. Gene **156**:119–122.

Nakamura, S., Mano, S., Tanaka, Y., Ohnishi, M., Nakamori, C., Araki, M., Niwa, T., Nishimura, M., Kaminaka, H., Nakagawa, T., et al. (2010). Gateway binary vectors with the bialaphos resistance gene, bar, as a selection marker for plant transformation. Biosci. Biotechnol. Biochem. **74**:1315–1319.

Nelissen, H., Eeckhout, D., Demuynck, K., Persiau, G., Walton, A., van Bel, M., Vervoort, M., Candaele, J., De Block, J., Aesaert, S., et al. (2015). Dynamic changes in ANGUSTIFOLIA3 complex composition reveal a growth regulatory mechanism in the maize leaf. Plant Cell **27**:1605–1619.

Ojolo, S.P., Cao, S., Priyadarshani, S.V.G.N., Li, W., Yan, M., Aslam, M., Zhao, H., and Qin, Y. (2018). Regulation of plant growth and development: a review from a chromatin remodeling perspective. Front. Plant Sci. **9**. https://doi.org/10.3389/fpls.2018.01232.

Pandey, R., Müller, A., Napoli, C.A., Selinger, D.A., Pikaard, C.S., Richards, E.J., Bender, J., Mount, D.W., and Jorgensen, R.A. (2002). Analysis of histone acetyltransferase and histone deacetylase families of *Arabidopsis thaliana* suggests functional diversification of chromatin modification among multicellular eukaryotes. Nucleic Acids Res. **30**:5036–5055.

Peirats-Llobet, M., Han, S.-K., Gonzalez-Guzman, M., Jeong, C.W., Rodriguez, L., Belda-Palazon, B., Wagner, D., and Rodriguez, P.L. (2016). A direct link between abscisic acid sensing and the chromatin-remodeling ATPase BRAHMA via core ABA signaling pathway components. Mol. Plant **9**:136–147.

Rao, R.S.P., Thelen, J.J., and Miernyk, J.A. (2014). In silico analysis of protein Lys-N(ε)-acetylation in plants. Front. Plant Sci. **5**:381.

Reyes, J.C. (2014). The many faces of plant SWI/SNF complex. Mol. Plant **7**:454–458.

Ritchie, M.E., Phipson, B., Wu, D., Hu, Y., Law, C.W., Shi, W., and Smyth, G.K. (2015). Limma powers differential expression analyses for RNA-sequencing and microarray studies. Nucleic Acids Res. **43**:e47.

Sacharowski, S.P., Gratkowska, D.M., Sarnowska, E.A., Kondrak, P., Jancewicz, I., Porri, A., Bucior, E., Rolicka, A.T., Franzen, R., Kowalczyk, J., et al. (2015). SWP73 subunits of *Arabidopsis* SWI/SNF chromatin remodeling complexes play distinct roles in leaf and flower development. Plant Cell **27**:1889–1906.

Sarnowska, E., Gratkowska, D.M., Sacharowski, S.P., Cwiek, P., Tohge, T., Fernie, A.R., Siedlecki, J.A., Koncz, C., and Sarnowski, T.J. (2016). The role of SWI/SNF chromatin remodeling complexes in hormone crosstalk. Trends Plant Sci. **21**:594–608.

Sarnowski, T.J., Ríos, G., Jásik, J., Swiezewski, S., Kaczanowski, S., Li, Y., Kwiatkowska, A., Pawlikowska, K., Koźbiał, M., Koźbiał, P., et al. (2005). SWI3 subunits of putative SWI/SNF chromatin-remodeling complexes play distinct roles during *Arabidopsis* development. Plant Cell **17**:2454–2472.

Shen, W., Xu, C., Huang, W., Zhang, J., Carlson, J.E., Tu, X., Wu, J., and Shi, Y. (2007). Solution structure of human Brg1 bromodomain and its specific binding to acetylated histone tails. Biochemistry **46**:2100–2110.

Shim, J.S., Kubota, A., and Imaizumi, T. (2017). Circadian clock and photoperiodic flowering in *Arabidopsis*: CONSTANS is a hub for signal integration. Plant Physiol. **173**:5–15.

Smaczniak, C., Immink, R.G.H., Muiño, J.M., Blanvillain, R., Busscher, M., Busscher-Lange, J., Dinh, Q.D.P., Liu, S., Westphal, A.H., Boeren, S., et al. (2012). Characterization of MADS-domain transcription factor complexes in *Arabidopsis* flower development. Proc. Natl. Acad. Sci. U S A **109**:1560–1565.

Sun, Z., Diaz, Z., Fang, X., Hart, M.P., Chesi, A., Shorter, J., and Gitler, A.D. (2011). Molecular determinants and genetic modifiers of aggregation and toxicity for the ALS disease protein FUS/TLS. PLoS Biol. **9**:e1000614.

Tian, T., Liu, Y., Yan, H., You, Q., Yi, X., Du, Z., Xu, W., and Su, Z. (2017). agriGO v2.0: a GO analysis toolkit for the agricultural community, 2017 update. Nucleic Acids Res. **45**:W122–W129.

Truebestein, L., and Leonard, T.A. (2016). Coiled-coils: the long and short of it. Bioessays News Rev. Mol. Cell. Dev. Biol. **38**:903–916.

Vercruyssen, L., Verkest, A., Gonzalez, N., Heyndrickx, K.S., Eeckhout, D., Han, S.-K., Jégu, T., Archacki, R., Van Leene, J., Andriankaja, M., et al. (2014). ANGUSTIFOLIA3 binds to SWI/SNF chromatin remodeling complexes to regulate transcription during *Arabidopsis* leaf development. Plant Cell **26**:210–229.

Ye, Y., Wu, H., Chen, K., Clapier, C.R., Verma, N., Zhang, W., Deng, H., Cairns, B.R., Gao, N., and Chen, Z. (2019). Structure of the RSC complex bound to the nucleosome. Science **366**:838–843.

Yu, Y., Liang, Z., Song, X., Fu, W., Xu, J., Lei, Y., Yuan, L., Ruan, J., Chen, C., Fu, W., et al. (2020). BRAHMA-interacting proteins BRIP1 and BRIP2 are core subunits of *Arabidopsis* SWI/SNF complexes. Nat. Plants **6**:996–1007.

Zhao, S., Zhang, B., Yang, M., Zhu, J., and Li, H. (2018). Systematic profiling of histone readers in *Arabidopsis thaliana*. Cell Rep. **22**:1090–1102.